A divergent CheW stabilizes nucleoid-associated chemosensory arrays

Annick Guiseppi[1*], Juan Jesus Vicente[2*], Aurelie Barneoud[1*], Audrey Moine[1], Leon Espinosa[1], Marie-Jeanne Basse[3], Virginie Molle[4], Tâm Mignot[1], Philippe Roche[3] and Emilia M.F. Mauriello[1#]

[1] Aix Marseille Univ, CNRS, LCB, Marseille, France; [2]Physiology & Biophysics, University of Washington, Seattle, WA, USA; [3]CNRS, INSERM, Aix Marseille Univ, Institute Paoli-Calmettes, CRCM, Marseille, France; [4]Montpellier II et I University, CNRS, Laboratoire de Dynamique des Interactions Membranaires Normales et Pathologiques, France.

[*] These authors contributed equally

[#]Correspondence to:
Emilia M.F. Mauriello
Aix Marseille Univ, CNRS, LCB
31 Chemin Joseph Aiguier, Marseille, 13402, France
Tel. +33491164321
Email : emauriello@imm.cnrs.fr

Running Title: The *Myxococcus xanthus* FrzB CheW-like protein acts upstream of the Frz chemotaxis pathway

SUMMARY

Chemosensory systems are highly organized signaling pathways allowing bacteria to adapt to environmental changes. The Frz chemosensory system from *M. xanthus* possesses, in addition to its core CheW, FrzA, a second CheW homologue, FrzB. We found that this protein does not interact with the cognate CheA, FrzE, as it lacks the amino acid region responsible of this interaction. FrzB, instead, acts upstream of FrzCD in the regulation of *M. xanthus* chemotaxis behaviors, and might function as an activator of the Frz pathway by physically stabilizing Frz nucleoid clusters. These results, together, show that the lack of the CheA-interacting region in FrzB confers new functions to this small protein.

INTRODUCTION

Chemosensory systems are specialized regulatory pathways that allow bacteria to perceive their external environment and respond with various cellular behaviors (Sourjik and Berg, 2002; Berleman and Bauer, 2005; Bible *et al.*, 2012). In these systems, environmental signals are transduced inside the cells initially by the aid of receptors also termed Methyl-accepting Chemotaxis Proteins (MCP). Most MCPs possess a transmembrane domain but 14% are soluble proteins (Collins *et al.*, 2014). Ligand-bound MCPs induce the autophosphorylation of the histidine kinase CheA that, in turn, transfers phosphoryl groups to at least two response regulators: CheY which is the most downstream component of the pathway and CheB which, together with CheR, constitutes the adaptation module. Che systems also include one or more of the docking protein CheW, interacting both with the C-terminal cytoplasmic tip of the MCP and with the P5 domain of CheA. CheW and $CheA^{P5}$ are paralogs and are topologically similar to SH3 domains from eukaryotic scaffold proteins that also play a role in signal transduction. Such domains are characterized by two intertwined 5-stranded β-barrels designated subdomain 1 and 2 (Bilwes *et al.*, 1999; Griswold *et al.*, 2002; Reebye *et al.*, 2012). MCP: $CheA^{P5}$: CheW interactions all involve subdomain 1 and 2. In particular, the β-barrels 3 and 4 of subdomain 1 of $CheA^{P5}$ interacts with the β-barrels 4 and 5 of subdomain 2 of CheW (Li *et al.*, 2013). The receptor cytoplasmic tip binds CheW or CheA at their hydrophobic junction between subdomain 1 and 2 (Li *et al.*, 2013).

High-resolution microscopy revealed that, intracellularly, Che proteins are organized in complex arrays running parallel to the bacterial inner membrane, with the MCP layer linked to a CheA/W baseplate (Khursigara *et al.*, 2008; Briegel *et al.*, 2009). Transversal views of these Che arrays show ordered MCP hexagons networked by CheA-CheW rings. CheA-CheW rings are composed of alternating and interacting $CheA^{P5}$ domains and CheWs. MCPs

hexagons are constituted by six MCP trimers of dimers. Each MCP in the dimer is connected with either a CheA^{P5} domain or a CheW, which allows connections between the MCP hexagons and the CheW-CheA^{P5} rings (Briegel *et al.*, 2012) (Fig. 1). The presence of each of these three proteins is essential for the integrity of the system (Sourjik and Berg, 2000; Wadhams *et al.*, 2005). This structure underlies the unique signaling properties of chemotaxis systems, including signal amplification and sensitivity (Sourjik and Berg, 2004; Ames and Parkinson, 2006; Li and Hazelbauer, 2014; Piñas *et al.*, 2016).

The gliding bacterium *M. xanthus* uses the cytoplasmic Frz signal transduction pathway to bias the frequency at which bacteria change their movement direction in response to environmental signals (Blackhart and Zusman, 1985). This chemotactic-like behavior might allow bacteria to glide towards favorable directions or away from toxic compounds. The Frz system induces a cell reversal by promoting the coordinate inversion of the cell polarity of the two *M. xanthus* motility systems: the Social (S) motility system powered by polar Type IV Pili and the Adventurous (A) motility powered by polarly assembled Agl-Glt complexes (Treuner-Lange *et al.*, 2015; Guzzo *et al.*, 2015; Chang *et al.*, 2016). The regulation of the motility systems by the Frz pathway is fundamental for cells to enter a developmental program that leads to the formation of multicellular fruiting bodies. The Frz core is composed of a cytoplasmic MCP (FrzCD), a CheA (FrzE) and a CheW (FrzA) (Bustamante *et al.*, 2004). In the absence of any of these three proteins cells display drastically reduced reversal frequencies and are not longer able to respond to the isoamyl alcohol (IAA), a Frz activator (Bustamante *et al.*, 2004; Guzzo *et al.*, 2015). The Frz system also includes a second CheW-like protein, FrzB described as an accessory because while in its absence cells show phenotypes similar to those caused by the deletion of core proteins, *ΔfrzB* cells are still able

to respond to IAA with increased reversal frequencies (Bustamante *et al.*, 2004; Guzzo *et al.*, 2015).

In this paper, we show that FrzB is a divergent CheW lacking the β-barrels involved in the interaction with the histidine kinase FrzE (β4 and β5). Strikingly, the introduction of β4 and β5 from FrzA to FrzB, converts the latter into a canonic CheW. Instead of mediating signal transduction from the FrzCD receptor to FrzE, FrzB acts upstream of FrzCD to activate cell reversals and stabilize the Frz chemosensory arrays at the nucleoid. Finally, the loss of the CheA-interacting region in FrzB might have been selected to provide an extra stabilizing module to nucleoid-associated chemosensory systems.

RESULTS

FrzB is upstream of the FrzCD receptor in the Frz signaling pathway

The first two genes of the *frz* operon encode the CheW-like proteins, FrzA and FrzB. *ΔfrzA* cells show the same motility and fruiting body formation phenotypes as *ΔfrzCD* and *ΔfrzE* suggesting that FrzA is the core CheW of the Frz pathway (McBride *et al.*, 1989; Bustamante *et al.*, 2004) (Fig. 2A). The aberrant behaviors at the colony level are due to the incapacity of *ΔfrzA* to modulate single cell reversal frequencies even in the presence of isoamyl alcohol (IAA), a known Frz activator (Fig. 2B) (Bustamante *et al.*, 2004; Guzzo *et al.*, 2015).

While a *frzB* deletion causes the same defects as *ΔfrzA* in the absence of IAA, IAA completely rescues the reversal frequency defect of *ΔfrzB* cells (Fig. 2B). This effect is detectable at both single cell and colony level (Fig. 2) (Bustamante *et al.*, 2004). These results show that signals from the FrzCD receptor can still be transduced to FrzE in the absence of FrzB and, thus, FrzB is not part of the Frz core.

Then, in order to determine the functional position of FrzB in the Frz pathway, we tested the epistasis of FrzB in respect to FrzCD. For this, we took advantage of a *frzCD* allele, *frzCDc*, whose expression confers a trans-dominant constitutively hyper-reversing phenotype (Fig. 2) (Bustamante et al., 2004) and constructed *ΔfrzA frzCDc* and *ΔfrzB frzCDc* double mutants. The *ΔfrzA frzCDc* reversal frequencies and colony phenotypes were identical to those of *ΔfrzA* cells, confirming that FrzA is located downstream of the receptor in the signaling pathway (Fig. 2). On the other hand, *ΔfrzB frzCDc* phenotypes resembled those of *frzCDc* (Fig. 2) indicating that FrzB is upstream of FrzCD in the Frz signaling pathway and that its requirement is bypassed by a constitutive frzCDc mutation.

FrzB does not interact with the downstream histidine kinase FrzE

Genetic data show that FrzB is upstream of FrzCD in the Frz regulatory pathway. We, thus, wanted to verify if FrzB could interact with FrzE. For this, we performed bacterial two-hybrid protein-protein interaction assays. As expected, both FrzA and FrzB interacted with FrzCD as well as with the FrzCD signaling domain alone ($FrzCD_{SD}$). On the other hand, only FrzA but not FrzB interacted with the FrzE-P5 domain ($FrzE^{P5}$) (Fig. 3A). Neither FrzA nor FrzB could interact with the FrzCD N-terminal domain (Fig. 3A).

If FrzB does not interact with FrzE, it should not be able to promote the phosphorylation of FrzE kinase domain ($FrzE^{CheA}$) *in vitro*. In fact, it has been previously shown that the presence of both FrzCD and FrzA is strictly required to achieve the transfer of a phosphoryl group from ATP to the Histidine at position 49 of $FrzE^{CheA}$ *in vitro* (Inclán *et al.*, 2007) (Fig. 3A). As expected, when we replaced FrzA with FrzB in the mixture no phosphorylation was detected suggesting that FrzB cannot mediate the $FrzE^{CheA}$ autophosphorylation *in vitro* (Fig. 3A).

Next, we asked what prevented FrzB from interacting with FrzE. To address this question, we decided to generate 3D homology models of the $FrzE^{P4-P5}$:FrzA and $FrzE^{P4-P5}$:FrzB complexes based on the *T. maritima* $CheA^{P4-P5}$:CheW crystal structure (Fig. 3C) (Li *et al.*, 2013). The structural models predict that FrzB cannot interact with FrzE due to the lack of a 20 amino acid region forming the β-barrels 4 and 5 of subdomain 2 and corresponding exactly to the CheW region important for the CheW: $CheA^{P5}$ interaction (Fig. 3C and D) (Li *et al.*, 2013). On the other hand and consistently with the two-hybrid system results, FrzB is predicted to contain all the hydrophobic amino acids involved in its interaction with FrzCD (Fig. 3D).

To verify if the lack of the FrzE interacting region in FrzB was directly associated with the loss of the FrzB-FrzE interaction, we designed a chimeric FrzB protein carrying the β-barrels 4 and 5 from FrzA ($FrzB^{\beta4-\beta5}$). First, we tested if purified $FrzB^{\beta4-\beta5}$ was able to replace FrzA in our $FrzE^{CheA}$ phosphorylation *in vitro* assay. Strikingly, when $FrzB^{\beta4-\beta5}$ was the only CheW in the

reaction mixture, it promoted the $FrzE^{CheA}$ phosphorylation similarly to FrzA, thus acting as a CheW (Fig. 3B). The $FrzE^{CheA}$ phosphorylation levels were a direct consequence of the FrzCD activation state, because when we used the hyperactive $FrzCD^{c}$ allele in the place of its wild type version, we observed a higher level of phosphorylated $FrzE^{CheA}$ (Fig. 3B).

Then, to test whether $FrzB^{\beta4\text{-}\beta5}$ could replace FrzA *in vivo* as *in vitro*, we transferred the gene coding for $FrzB^{\beta4\text{-}\beta5}$ in a *ΔfrzA ΔfrzB* strain at the endogenous locus. $FrzB^{\beta4\text{-}\beta5}$ was stably expressed (Supporting Information Figure S1A) and the resulting strain had phenotypes and reversal frequencies similar to those of *ΔfrzB* both in the presence and in the absence of IAA (Fig. 2). These results suggest that *in vivo,* like *in vitro*, $FrzB^{\beta4\text{-}\beta5}$ can connect FrzCD to FrzE, like FrzA.

FrzB is an activator of the Frz pathway

Because FrzB does not interact with FrzE, we wanted to explore the possibility, also suggested by genetic results, that FrzB acted directly on the FrzCD receptor to deliver some yet unknown signals and activate the Frz system. We reasoned that if this were true, the overexpression of FrzB would cause a hyper-activation of the Frz system and increased reversal frequencies. To verify this hypothesis, we cloned *frzB* on a replicative plasmid under the control of the constitutive strong *pilA* promoter (Zhao *et al.*, 2008) and transformed wild type cells with the resulting plasmid. The resulting strain overexpresses FrzB (Supporting Information Figure S1A). When we measured the reversal frequencies of cells of this strain, they showed a significantly higher number of reversals per hour as compared to wild type (Fig. 4A). Increased reversals also prevented cells from producing a net swarming at the colony level and fruiting bodies analogously to a constitutively active Frz mutant ($frzCD^{c}$) (compare Fig. 4B and Fig. 2B).

To check if this effect was specific of FrzB, we constructed a strain overexpressing FrzA (Supporting Information Figure S1B). This strain had wild type reversal frequencies and colony phenotypes (Fig. 4). In light of these results, we propose that FrzB might be an activator of the Frz system acting directly on the FrzCD receptor.

FrzB might be a stabilizing factor of Frz signaling arrays

It has been previously shown that Frz proteins form nucleoid associated signaling complexes (Kaimer and Zusman, 2016; Moine *et al.*, 2017). To verify whether FrzB was part of the Frz clusters, we constructed a *mCherry-frzB* fusion that replaced *frzB* at the endogenous locus and encoded a functional protein (Supporting Information Figure S1 and Supporting Information Figure S2). mCherry-FrzB formed multiple-nucleoid associated clusters that resembled those formed by FrzCD-GFP and FrzE-mCherry (Fig. 5A) (Moine *et al.*, 2017), suggesting that the three proteins are part of the same complexes.

Then, we decided to check how the absence of FrzA and FrzB affected the formation of these complexes. For that, we transferred a functional *frzE-mCherry* gene fusion (Moine *et al.*, 2017) in the *ΔfrzA* and *ΔfrzB* mutants. *M. xanthus* cells of the resulting strains were then spotted on agar pads and imaged by fluorescence microscopy. Fig. 5B shows that while FrzE-mCherry was completely dispersed in the cytoplasm in the absence of FrzA, the fusion protein retained its ability to assemble multiple nucleoid-associated clusters in the absence of FrzB. Neverthless, in *ΔfrzB* cells, Frz clusters were not well defined and intense as in wild type (Fig. 5B) suggesting that even if FrzB is not required for the formation of Frz chemosensory arrays at the nucleoid, it is important for their stability. The aberrant localization patterns were not due to a change in the FrzE-mCherry protein levels (Supporting Information Figure S3).

DISCUSSION

Chemosensory systems are modified two component systems where the addition of accessory proteins confers unique properties like signal amplification and sensitivity. In this work, we found that the CheW-like protein FrzB lacks a 20 amino acid sequence corresponding to two β-barrels that in chemosensory systems are important for CheA:CheW interactions (Li *et al.*, 2013:2). Thus, FrzB cannot interact with FrzE and mediate its autophosphorylation. The loss of this protein region might have been selected to confer to this small protein the unique function of activating and stabilizing nucleoid Frz chemosensory arrays. How would FrzB accomplish these tasks? It has been shown that Che arrays are constituted by hexagons of MCP trimers of dimers networked by Che^{P5}-CheW rings (Briegel *et al.*, 2012). However, if FrzB cannot interact with $FrzE^{P5}$, it cannot participate to the formation of Che^{P5}-CheW rings either. It has been proposed that in addition to Che^{P5}-CheW rings, Che networks also have six-member CheW rings that only interact with the MCPs (Fig. 1) and whose role remains to be elucidated (Liu *et al.*, 2012; Piñas *et al.*, 2016). We can imagine that FrzB forms this kind of rings whose function could be to ensure array activation and stability (Fig. 1). Indeed, for the correct activation and stabilization of chemosensory arrays at the nucleoid an extra stabilizing factor might be required. Such stabilizing factor would be dispensable when receptors arrays are tightly embedded in the inner membrane. A case analogous to the one proposed is represented by the *V. cholerae* cytoplasmic chemotaxis cluster 1, whose stabilization is guarantied by the presence of an additional signaling domain in its DosM receptor (Briegel *et al.*, 2016).

Interestingly, the FrzCD receptor does not contain an obvious signal-binding domain. Instead, it contains an N-terminal region that has been recently shown to be involved in DNA binding (Moine *et al.*, 2017). Thus, a second FrzB function could be to deliver signals to the

Frz pathway. FrzB could bind directly some cytoplasmic molecules and transduce signals to FrzCD, thus, functioning as a sensor of the cellular metabolic state. However, FrzB could also connect FrzCD to another MCP or sensor kinase. *M. xanthus* encodes a total of 21 MCPs (Moine *et al.*, 2014). Among them, only Mcp7 is cytoplasmic like FrzCD, but its localization strongly excludes an association with the Frz pathway (Moine *et al.*, 2014). We could imagine that FrzCD, which forms clusters on the nucleoid (Kaimer and Zusman, 2016; Moine *et al.*, 2017), could associate with a transmembrane MCP or sensor kinase at regions where the nucleoid surface is particularly close to the inner membrane (Adams *et al.*, 2015). In fact, previous works show the association of FrzCD with membrane fractions (McBride *et al.*, 1992) as well as interactions with envelop-associated A-motility proteins (Mauriello *et al.*, 2009; Nan *et al.*, 2010). The hypothesis that FrzB is a Frz input does not rule out that FrzCD itself can somehow bind signals. Indeed, FrzCD responds to IAA independently on FrzB (Fig. 2).

In the last years, the discovery of different accessories Che proteins allowed the identification of new functions and degrees of complexity in the regulation of the cellular responses operated by chemosensory systems. By unraveling a new accessory protein and its function, this work open new insights on the knowledge of the regulatory potentials of bacterial chemosensory systems.

EXPERIMENTAL PROCEDURES

Bacterial strains, plasmids and growth

*S*trains and plasmids are listed in Table 1 and 2, respectively. *M. xanthus* strains were grown at 32°C in CYE rich media as previously described.

Plasmids were introduced into *M. xanthus* cells by electroporation. Deletions and GFP fusions were inserted in frame, using the pBJ113 or pBJ114 vectors, to avoid polar effects on the downstream gene expression (Bustamante *et al.*, 2004; Moine *et al.*, 2014).

Strains EM538 and EM539 were obtained by deleting *frzA* from codon 15 to 145 and *frzB* from codon 11 to 92, respectively. In both strains we also deleted *frzCD* from codon 6 to 182.

To construct plasmid pEM399 to generate EM515, a DNA fragment was generated by PCR overlapping a DNA region amplified with primers CCCAAGCTTCTTCAGCTCGAGGCTGGCAA and TGCCCCTTGCTCACCATCTCCTCCTCCTTCTCATGGAA and *mCherry* amplified with primers CATGAGAAGGAGGAGGAGATGGTGAGCAAGGGCGAGGA and CGGGATCCTCTAGACTTGCACAGCTCGTCCATGC from pEM147 (Mauriello *et al.*, 2009). This fusion product was digested with HindIII and BamHI. *frzB* was amplified with primers CGGGATCCGGAGCAGGAGACCTCCTCTTCTTCGACAT and GGAATTCGCGGACGAGGACAGCCTCAA and digested with BamHI and EcoRI. The two fragments were then cloned into pBJ113 previously digested with HindIII and BamHI in a three-partner ligation reaction.

To obtain strains EM455 and EM458, plasmid pEM365 was transferred into strains DZ4479 and DZ4478 respectively.

For the construction of $frzB^{\beta4\text{-}\beta5}$ we replaced codon 27 to 36 of FrzB with codon 41 to 75 of FrzA. Plasmids pEM605 and pEM464 were synthesized by Biomatik.

To construct plasmids pEM442 and pEM393, we first constructed plasmid pJV101 by cloning the pilA promoter region, previously amplified with primers cctctagaagcccgggagcgcttcggatgcgta and cctctagagaatcgcgagacgcgcatgggggtc and cloned into plasmid pZJV41 (Zhao *et al.*, 2008) at the XbaI site. Then, we amplified *frzB* with primers GGGGTACCAAGGAGGAGGAGGTGGACCTCC and GGAATTCTCAGTGCCTTCCTTGAGTCCTT and *frzA* with primers CGGGTACCCGAGCACTCCGGATGGCTC and GGGAATTCTCACCGCGCCACCGCCCGCTG. The PCR products were then digested with KpnI and EcoRI and cloned it in pJV101 previously digested with the same enzymes.

Escherichia coli cells were grown under standard laboratory conditions in Luria-Bertani broth supplemented with antibiotics if necessary.

For swarming and fruiting body assays, cells (5 µl) at a concentration of 5×10^{9} cfu ml^{-1} were spotted on CYE or CF (for fruiting body formation) agar plates and incubated at 32°C and photographed after respectively 48h or 72h with an Olympus SZ61 binocular stereoscope.

Reversal frequencies

5 µl of cells from 4 x 10^{8} cfu ml^{-1} vegetative CYE cultures were spotted on a thin fresh TPM agar supplied or not with 0.15 % IAA. Time-lapse movies were shot for 1 hour with frames captured every 30 seconds. Movies were obtained and reversal frequencies calculated with Image J (Rasband, W.S., ImageJ, U. S. National Institutes of Health, Bethesda, Maryland, USA, http://imagej.nih.gov/ij/, 1997-2012) and FIJI as previously described (Guzzo *et al.*, 2015). The reversal frequencies distributions were obtained with the R software (https://www.r-project.org/). Statistical significance was obtained with a Wilcox Test from R.

Bacterial two-hybrid experiments

Bacterial two-hybrid experiments were performed on plates as previously described (Moine *et al.*, 2014) and as recommended by the manufacturer instructions (Euromedex).

Sequence alignment and homology modeling

Predictions of secondary structures and protein sequence alignments were obtained with Jpred (Cole *et al.*, 2008) and Clustal Omega (Sievers and Higgins, 2014), respectively. Homology models of FrzA (Uniprot P43498) or FrzB (Uniprot P43499) in the presence of FrzE (Uniprot P18769) were built with MODELLER 9v12 (Webb and Sali, 2016). Crystal structure of the complex between bacterial chemotaxis histidine kinase $CheA^{P4-P5}$ and receptor-adaptor protein CheW (PDB codes 2CH4) was used as template (Park *et al.*, 2006). The modeling was performed in a two-step manner: First, each individual domain was modeled separately using the 3D structure of its *T. maritima* counterpart as a template. CheW (2CH4 chain W) was used to build models of FrzA and FrzB. The N terminal domain of CheA (2CH4 chain A resid 355-540) and the C terminal domain of CheA (2CH4 chain A resid 541-671) were used to build N and C terminal domains of FrzE. In a second step, each model was superimposed to its counterpart in the x-ray structure of the CheW-CheA complex (chains W and A). The Frz proteins exhibit high enough identities to their Che counterparts to build reasonable 3D models. FrzB vs CheW (26.1% identity, 45% similarity), FrzA vs CheW (26.6% identity, 46.7% similarity), $FrzE^{p4}$ vs. $CheA^{p4}$ (46.5% identity, 71.7% similarity), $FrzE^{p5}$ vs. $CheA^{p5}$ (26.1% identity, 53.8% similarity). Quality of the models was assessed with Prosess server (http://www.prosess.ca). Structural alignments were performed with Protein structure comparison service PDBeFold at European Bioinformatics Institute (http://www.ebi.ac.uk/msd-srv/ssm) (Krissinel and Henrick, 2004). Fig. 3C showing the

lowest energy model was generated with pymol (http://pymol.org). Fig. 3D was generated with ESPript web server (Gouet *et al.*, 2003).

Fluorescence microscopy and image analysis

For fluorescence microscopy analyses, 5 ml of cells from 4 x 10^8 cfu ml^{-1} vegetative CYE cultures were spotted on a thin fresh TPM agar pad at the top a slide (Mignot *et al.*, 2005). A cover slip was added immediately on the top of the pad, and the obtained slide was analyzed by microscopy using a Nikon Eclipse TE2000 E PFS inverted epifluorescence microscope (100 x oil objective NA 1.3 Phase Contrast) (Ducret *et al.*, 2009).

To study the colocalization with the DNA, the TPM agar pads were supplied with 1µg ml^{-1} DAPI stain. FrzB clusters, nucleoid areas and cell areas were automatically detected and verified manually with the "MicrobeJ" Fiji/ImageJ plugin created by A. Ducret, Brun Lab (http://www.indiana.edu/~microbej/index.html). All data plots and statistical tests were obtained with the R software (https://www.r-project.org/).

***In vitro* autophosphorylation assay**

In vitro phosphorylation assays were performed with *E. coli* purified recombinant proteins. 4 µg of $FrzE^{CheA}$ were incubated with 1µg of FrzA, FrzB or $FrzB^{\beta4\text{-}\beta5}$ and FrzCD or $FrzCD^{c}$ in 25 µl of buffer P (50 mM Tris-HCl, pH 7.5; 1 mM DTT; 5 mM $MgCl_2$; 50mM KCl; 5 mM EDTA; 50µM ATP, 10% glycerol) supplemented with 200 µCi ml^{-1} (65 nM) of [γ-33P]ATP (PerkinElmer, 3000 Ci $mmol^{-1}$) for 10 minutes at room temperature in order to obtain the optimal $FrzE^{CheA}$ autophosphorylation activity. Each reaction mixture was stopped by addition of 5 × Laemmli and quickly loaded onto SDS-PAGE gel. After electrophoresis, proteins were

revealed using Coomassie Brilliant Blue before gel drying. Radioactive proteins were visualized by autoradiography using direct exposure to film (Carestream).

Acknowledgements

Research on chemotaxis in our laboratory is funded by the Agence National de la Recherche

Jeune Chercheur-Jeune Chercheuse (ANR-14-CE11-0023-01) to E.M.M.

References

Adams, D.W., Wu, L.J., and Errington, J. (2015) Nucleoid occlusion protein Noc recruits DNA to the bacterial cell membrane. *EMBO J* **34**: 491–501.

Ames, P., and Parkinson, J.S. (2006) Conformational suppression of inter-receptor signaling defects. *Proc Natl Acad Sci U S A* **103**: 9292–9297.

Berleman, J.E., and Bauer, C.E. (2005) Involvement of a Che-like signal transduction cascade in regulating cyst cell development in Rhodospirillum centenum. *Mol Microbiol* **56**: 1457–1466.

Bible, A., Russell, M.H., and Alexandre, G. (2012) The Azospirillum brasilense Che1 chemotaxis pathway controls swimming velocity, which affects transient cell-to-cell clumping. *J Bacteriol* **194**: 3343–3355.

Bilwes, A.M., Alex, L.A., Crane, B.R., and Simon, M.I. (1999) Structure of CheA, a signal-transducing histidine kinase. *Cell* **96**: 131–141.

Blackhart, B.D., and Zusman, D.R. (1985) “Frizzy” genes of Myxococcus xanthus are involved in control of frequency of reversal of gliding motility. *Proc Natl Acad Sci U S A* **82**: 8767–8770.

Briegel, A., Li, X., Bilwes, A.M., Hughes, K.T., Jensen, G.J., and Crane, B.R. (2012) Bacterial chemoreceptor arrays are hexagonally packed trimers of receptor dimers networked by rings of kinase and coupling proteins. *Proc Natl Acad Sci U S A* **109**: 3766–3771.

Briegel, A., Ortega, D.R., Mann, P., Kjær, A., Ringgaard, S., and Jensen, G.J. (2016) Chemotaxis cluster 1 proteins form cytoplasmic arrays in Vibrio cholerae and are stabilized by a double signaling domain receptor DosM. *Proc Natl Acad Sci U S A* **113**: 10412–10417.

Briegel, A., Ortega, D.R., Tocheva, E.I., Wuichet, K., Li, Z., Chen, S., *et al.* (2009) Universal architecture of bacterial chemoreceptor arrays. *Proc Natl Acad Sci U S A* **106**: 17181–17186.

Bustamante, V.H., Martinez-Flores, I., Vlamakis, H.C., and Zusman, D.R. (2004) Analysis of the Frz signal transduction system of Myxococcus xanthus shows the importance of the conserved C-terminal region of the cytoplasmic chemoreceptor FrzCD in sensing signals. *Mol Microbiol* **53**: 1501–13.

Chang, Y.-W., Rettberg, L.A., Treuner-Lange, A., Iwasa, J., Søgaard-Andersen, L., and Jensen, G.J. (2016) Architecture of the type IVa pilus machine. *Science* **351**: aad2001.

Cole, C., Barber, J.D., and Barton, G.J. (2008) The Jpred 3 secondary structure prediction server. *Nucleic Acids Res* **36**: W197–W201.

Collins, K.D., Lacal, J., and Ottemann, K.M. (2014) Internal sense of direction: sensing and signaling from cytoplasmic chemoreceptors. *Microbiol Mol Biol Rev MMBR* **78**: 672–684.

Ducret, A., Maisonneuve, E., Notareschi, P., Grossi, A., Mignot, T., and Dukan, S. (2009) A microscope automated fluidic system to study bacterial processes in real time. *PloS One* **4**: e7282.

Gouet, P., Robert, X., and Courcelle, E. (2003) ESPript/ENDscript: extracting and rendering sequence and 3D information from atomic structures of proteins. *Nucleic Acids Res* **31**: 3320–3323.

Griswold, I.J., Zhou, H., Matison, M., Swanson, R.V., McIntosh, L.P., Simon, M.I., and Dahlquist, F.W. (2002) The solution structure and interactions of CheW from Thermotoga maritima. *Nat Struct Biol* **9**: 121–125.

Guzzo, M., Agrebi, R., Espinosa, L., Baronian, G., Molle, V., Mauriello, E.M.F., *et al.* (2015) Evolution and Design Governing Signal Precision and Amplification in a Bacterial Chemosensory Pathway. *PLoS Genet* **11**: e1005460.

Inclán, Y.F., Vlamakis, H.C., and Zusman, D.R. (2007) FrzZ, a dual CheY-like response regulator, functions as an output for the Frz chemosensory pathway of Myxococcus xanthus. *Mol Microbiol* **65**: 90–102.

Kaimer, C., and Zusman, D.R. (2016) Regulation of cell reversal frequency in Myxococcus xanthus requires the balanced activity of CheY-like domains in FrzE and FrzZ. *Mol Microbiol* **100**: 379–395.

Khursigara, C.M., Wu, X., and Subramaniam, S. (2008) Chemoreceptors in Caulobacter crescentus: trimers of receptor dimers in a partially ordered hexagonally packed array. *J Bacteriol* **190**: 6805–6810.

Krissinel, E., and Henrick, K. (2004) Secondary-structure matching (SSM), a new tool for fast protein structure alignment in three dimensions. *Acta Crystallogr D Biol Crystallogr* **60**: 2256–2268.

Li, M., and Hazelbauer, G.L. (2014) Selective allosteric coupling in core chemotaxis signaling complexes. *Proc Natl Acad Sci U S A* **111**: 15940–15945.

Li, X., Fleetwood, A.D., Bayas, C., Bilwes, A.M., Ortega, D.R., Falke, J.J., *et al.* (2013) The 3.2 Å resolution structure of a receptor: CheA:CheW signaling complex defines overlapping binding sites and key residue interactions within bacterial chemosensory arrays. *Biochemistry (Mosc)* **52**: 3852–3865.

Liu, J., Hu, B., Morado, D.R., Jani, S., Manson, M.D., and Margolin, W. (2012) Molecular architecture of chemoreceptor arrays revealed by cryoelectron tomography of Escherichia coli minicells. *Proc Natl Acad Sci U S A* **109**: E1481-1488.

Mauriello, E.M.F., Nan, B., and Zusman, D.R. (2009) AglZ regulates adventurous (A-) motility in Myxococcus xanthus through its interaction with the cytoplasmic receptor, FrzCD. *Mol Microbiol* **72**: 964–977.

McBride, M.J., Köhler, T., and Zusman, D.R. (1992) Methylation of FrzCD, a methyl-accepting taxis protein of Myxococcus xanthus, is correlated with factors affecting cell behavior. *J Bacteriol* **174**: 4246–4257.

McBride, M.J., Weinberg, R.A., and Zusman, D.R. (1989) "Frizzy" aggregation genes of the gliding bacterium Myxococcus xanthus show sequence similarities to the chemotaxis genes of enteric bacteria. *Proc Natl Acad Sci U S A* **86**: 424–428.

Mignot, T., Merlie, J.P., and Zusman, D.R. (2005) Regulated pole-to-pole oscillations of a bacterial gliding motility protein. *Science* **310**: 855–7.

Moine, A., Agrebi, R., Espinosa, L., Kirby, J.R., Zusman, D.R., Mignot, T., and Mauriello, E.M.F. (2014) Functional organization of a multimodular bacterial chemosensory apparatus. *PLoS Genet* **10**: e1004164.

Moine, A., Espinosa, L., Martineau, E., Yaikhomba, M., Jazleena, P.J., Byrne, D., *et al.* (2017) The nucleoid as a scaffold for the assembly of bacterial signaling complexes. *bioRxiv* 169912.

Nan, B., Mauriello, E.M.F., Sun, I.-H., Wong, A., and Zusman, D.R. (2010) A multi-protein complex from Myxococcus xanthus required for bacterial gliding motility. *Mol Microbiol* **76**: 1539–1554.

Park, S.-Y., Borbat, P.P., Gonzalez-Bonet, G., Bhatnagar, J., Pollard, A.M., Freed, J.H., *et al.* (2006) Reconstruction of the chemotaxis receptor-kinase assembly. *Nat Struct Mol Biol* **13**: 400–407.

Piñas, G.E., Frank, V., Vaknin, A., and Parkinson, J.S. (2016) The source of high signal cooperativity in bacterial chemosensory arrays. *Proc Natl Acad Sci U S A* **113**: 3335–3340.

Reebye, V., Frilling, A., Hajitou, A., Nicholls, J.P., Habib, N.A., and Mintz, P.J. (2012) A perspective on non-catalytic Src homology (SH) adaptor signalling proteins. *Cell Signal* **24**: 388–392.

Sievers, F., and Higgins, D.G. (2014) Clustal omega. *Curr Protoc Bioinforma Ed Board Andreas Baxevanis Al* **48**: 3.13.1-16.

Sourjik, V., and Berg, H.C. (2000) Localization of components of the chemotaxis machinery of Escherichia coli using fluorescent protein fusions. *Mol Microbiol* **37**: 740–751.

Sourjik, V., and Berg, H.C. (2002) Binding of the Escherichia coli response regulator CheY to its target measured in vivo by fluorescence resonance energy transfer. *Proc Natl Acad Sci U S A* **99**: 12669–12674.

Sourjik, V., and Berg, H.C. (2004) Functional interactions between receptors in bacterial chemotaxis. *Nature* **428**: 437–441.

Treuner-Lange, A., Macia, E., Guzzo, M., Hot, E., Faure, L.M., Jakobczak, B., *et al.* (2015) The small G-protein MglA connects to the MreB actin cytoskeleton at bacterial focal adhesions. *J Cell Biol* **210**: 243–256.

Wadhams, G.H., Martin, A.C., Warren, A.V., and Armitage, J.P. (2005) Requirements for chemotaxis protein localization in Rhodobacter sphaeroides. *Mol Microbiol* **58**: 895–902.

Webb, B., and Sali, A. (2016) Comparative Protein Structure Modeling Using MODELLER. *Curr Protoc Bioinforma Ed Board Andreas Baxevanis Al* **54**: 5.6.1-5.6.37.

Zhao, J., Zhong, L., Shen, M., Xia, Z., Cheng, Q., Sun, X., *et al.* (2008) Discovery of the Autonomously Replicating Plasmid pMF1 from Myxococcus fulvus and Development of a Gene Cloning System in Myxococcus xanthus. *Appl Environ Microbiol* **74**: 1980–1987.

1 **FIGURE LEGEND**

2 **Fig. 1.** MCP form trimers of dimers (each dimer is shown as a green circle), which, in turn,
3 form hexagons connected with rings composed of the CheA-P5 domain (dark blue bars) and
4 CheW (white bars). A signaling unit is represented in the red box. The blue circles represent
5 CheA-P4 domains. 6CheW-rings (shown at the center of the array) might serve to modulate
6 the system stability and thus activation.

7

8 **Fig. 2.** FrzB is not required for the IAA response and is upstream to FrzCD. (A) Motility and
9 fruiting body formation phenotypes were photographed at 48h and 72h, respectively. A
10 motility phenotypes were verified by introducing a *pilA::tet* mutation in each strain. (B) Box
11 plots of reversal frequencies of single cells moving on agar pads supplemented or not with
12 0,15% IAA.

13

14 **Fig. 3.** FrzB interacts with FrzCD but not with FrzE. (A) Bacterial two-hydrid assays on plates.
15 Interactions between the indicated Frz proteins are shown: (+) indicates bacterial colonies
16 turning red within 24h or 48h; (-) means that the colony color was as the negative control;
17 ND stands for "not determined". We only show interactions reproducible in two
18 experiments performed in triplicate. Examples of colonies from negative control (empty
19 plasmids) and (pKT25C*mcpM*/pUT18C*cheW4b* from Moine *et al.*, 2014) are shown. (B) The
20 $FrzB^{\beta4\text{-}\beta5}$ chimera can promote FrzE phosphorylation. Kinetics of the FrzE kinase domain
21 ($FrzE^{CheA}$) auto-phosphorylation were tested *in vitro* by incubation of $FrzE^{CheA}$ in the presence
22 of FrzA, FrzB or $FrzB^{\beta4\text{-}\beta5}$, the indicated different forms of FrzCD and $ATP\gamma P^{33}$ as a phosphate
23 donor. (C) 3D models of the $FrzE^{P4\text{-}P5}$:FrzA and $FrzE^{P4\text{-}P5}$:FrzB complexes based on the *T.*
24 *maritima* $CheA^{P4\text{-}P5}$:CheW crystal structure (PDB 2ch4). The 20 amino acid region forming the

1 β-barrels 4 and 5 of subdomain 2 and corresponding to the CheW region important for the
2 CheW:CheA^{P5} interaction are highlighted in red in the FrzA structure. These residues are
3 missing in FrzB. (D) Protein structural alignments between *T. maritima* CheW x-ray structure
4 and *M. xanthus* FrzA and FrzB theoretical 3D models. CheW residues in atomic contact with
5 CheA and MCP are shown as red stars and blue squares respectively. Secondary structures
6 determined from CheW x-ray structure are shown on top of the alignment.

7

8 **Fig. 4.** FrzB overexpression causes increased reversals. (A) Box plots of reversal frequencies
9 of single cells moving on agar pads. The star indicates that the reversal frequencies of strain
10 *pJV101 pilA::frzB*$^{\beta4\text{-}\beta5}$ are significantly different from the other plotted strains (P < 5e-05). P
11 values are further detailed in Table 3. (B) Motility and fruiting body formation phenotypes
12 were photographed at 48h and 72h, respectively.

13 **Fig. 5.** FrzB-mcherry colocalizes with the nucleoid in *M. xanthus*. (A) (Right) Micrographs of
14 *mcherry-frzB* cells stained with the DNA DAPI stain. (Middle) mCherry (red) and DAPI
15 fluorescence (blue) profiles are shown with the fluorescence intensity (arbitrary units)
16 represented on the *y*-axis and the cell length positions with -1 and +1 indicating the poles,
17 on the *x*-axis. (Left) Correlation coefficients between the DAPI and mCherry localization are
18 plot. R^2 values > 0,5 indicate significant correlations. The table compares the R^2 values
19 between the indicated fluorescent fusion and DAPI staining. (B) (Right) Fluorescence
20 micrographs of the indicated *M. xanthus* strains carrying a FrzE-mCherry fusion. (Middle)
21 mCherry (red) fluorescence profiles are represented as in (A). (Left) 265 cells for *frzE-*
22 *mCherry* and 296 cells for *frzE-mCherry ΔfrzB* issued from a biological replicate, are ordered

according to their cell length (pixels) and for each cell the mCherry fluorescence is represented as red dots at their corresponding cell position. 0 is the cell center.

1 **SUPPLEMENTARY FIGURE LEGEND**

2 **Supporting Information Figure S1.** Western blot with anti-FrzB (A) or anti-FrzA antibodies (B)
3 on the cell extracts of the indicated *M. xanthus* strains. White lines are used to indicate that
4 two lanes from the same gel were separated by other lanes.

5

6 **Supporting Information Figure S2.** Phenotypic assays of the indicated strains.

7

8 **Supporting Information Figure S3.** Western blot with anti-FrzE antibodies on the cell
9 extracts of the indicated *M. xanthus* strains.

10

11

12

Table 1. Strain list

Strains	Genotype	Reference or source
DZ2	*wt*	Zusman et al., 1982
DZ4478	*ΔfrzA*	Bustamante et al ; 2004
DZ4479	*ΔfrzB*	Bustamante et al ; 2004
DZ4487	*frzCDΔ6-182*	Bustamante et al ; 2004
EM538	*ΔfrzA frzCDΔ6-182*	This study
EM539	*ΔfrzB frzCDΔ6-182*	This study
EM434	*frzE-mCherry*	Moine et al., 2016
EM455	*ΔfrzB frzE-mCherry*	This study
EM458	*ΔfrzA frzE-mCherry*	This study
EM515	*frzB-mCherry*	This study
EM605	*ΔfrzA ΔfrzB* $frzB^{\beta4\text{-}\beta5}$	This study

Table 2. Plasmid list

Plasmid	Expression plasmid	Source
pEM411	pBJ113 with construct for *ΔfrzA frzCDΔ6-182*	This study
pEM412	pBJ113 with construct for *ΔfrzB frzCDΔ6-182*	This study
pEM365	pBJ113 with construct for *frzE-mCherry*	Moine et al., 2016
pEM399	pBJ113 with construct for *frzB-mCherry*	This study
pEM463	pBJ113 with construct *ΔfrzA ΔfrzB* $frzB^{\beta4\text{-}\beta5}$ (Biomatik)	This study
pZJV41		(Zhao *et al.*, 2008)
pJV101	pZJV41 with *pilA* promoter	This study
pEM393	pJV101 *frzB*	This study
pEM442	pJV101 *frzA*	This study
pEM443	pKT25 with *frzA*	This study
pEM391	pKTN25 with *frzB*	This study
pEM369	pKTN25 with *frzCDΔ6-130*	This study
pEM370	pKTN25 with *frzCDΔ143-417*	This study
pEM371	pKTN25 with *frzCD*	This study
pEM372	pKTN25 with *frzEΔ1-511/646-777*	This study
pEM379	pUT18C *frzA*	This study
pEM392	pUT18 *frzB*	This study
pEM381	pUT18C with *frzCDΔ6-130*	This study
pEM382	pUT18C with *frzCDΔ143-417*	This study
pEM382	pUT18C with *frzCD*	This study
pEM382	pUT18C with *frzEΔ1-511/646-777*	This study
pETPhos *frzCD*	pETPhos with *frzCD* tagged with 6-his inducible with IPTG	Guzzo et al., 2015
pETPhos $frzE^{P5}$	pETPhos with $frzE^{kinase}$ tagged with 6-his inducible with IPTG	Guzzo et al., 2015
pETPhos $frzCD^{c}$	pETPhos with $frzCD^{c}$ tagged with 6-his inducible with IPTG	Guzzo et al., 2015
pGEX(M) *frzA*	pETPhos with *frzA* tagged with 6-his inducible with IPTG	Guzzo et al., 2015
pETPhos *frzB*	pETPhos with *frzB* tagged with 6-his inducible with IPTG	This study
pEM464	pETPhos with $frzB^{\beta4\text{-}\beta5}$ tagged with 6-his inducible with IPTG (Biomatik)	This study

Table 3. P values (Wilcox test) for Fig. 2B

	wt	pJV101	SurB	SurA	SurAB
wt		0,08	2,20E-16	0,27	0,73
pJV101	0,08		2,70E-15	0,74	0,08
SurB	2,20E-16	2,70E-15		4,90E-05	1,16E-14
SurA	0,27	0,74	4,90E-05		0,28
SurAB	0,73	0,08	1,16E-14	0,28	

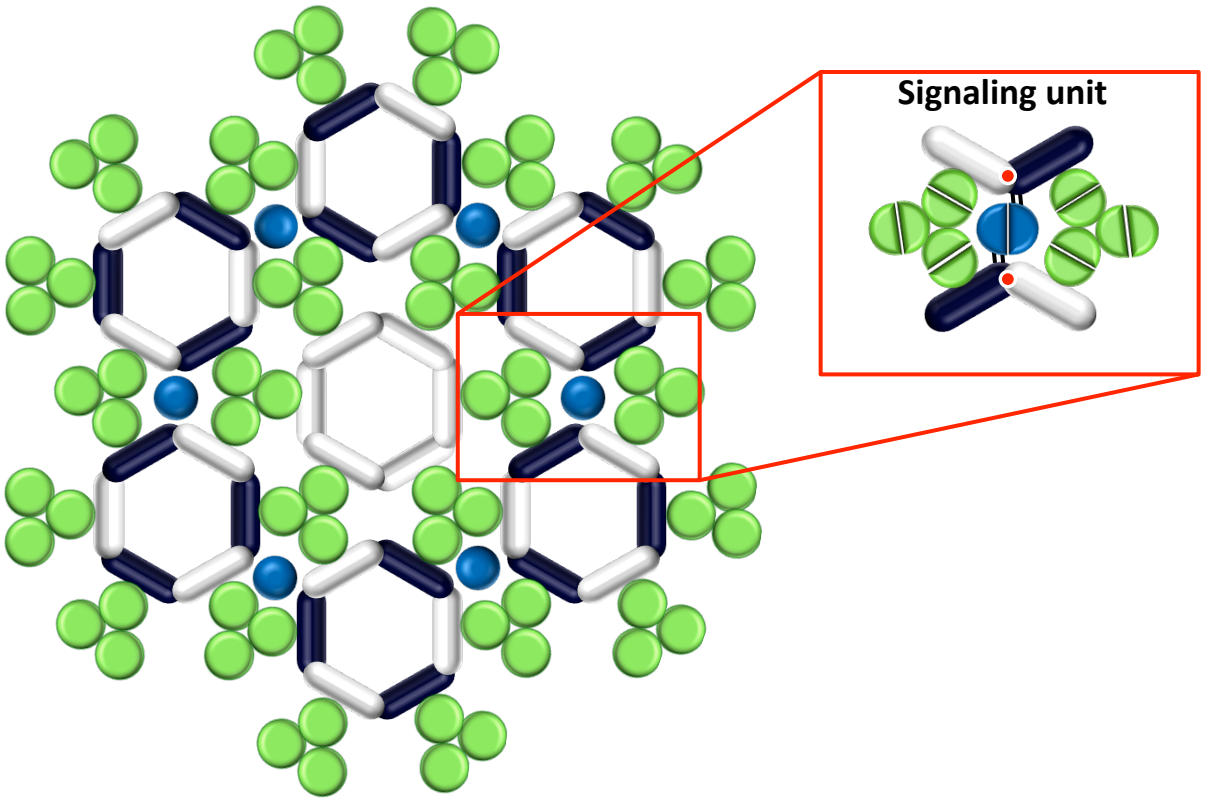
Signaling unit

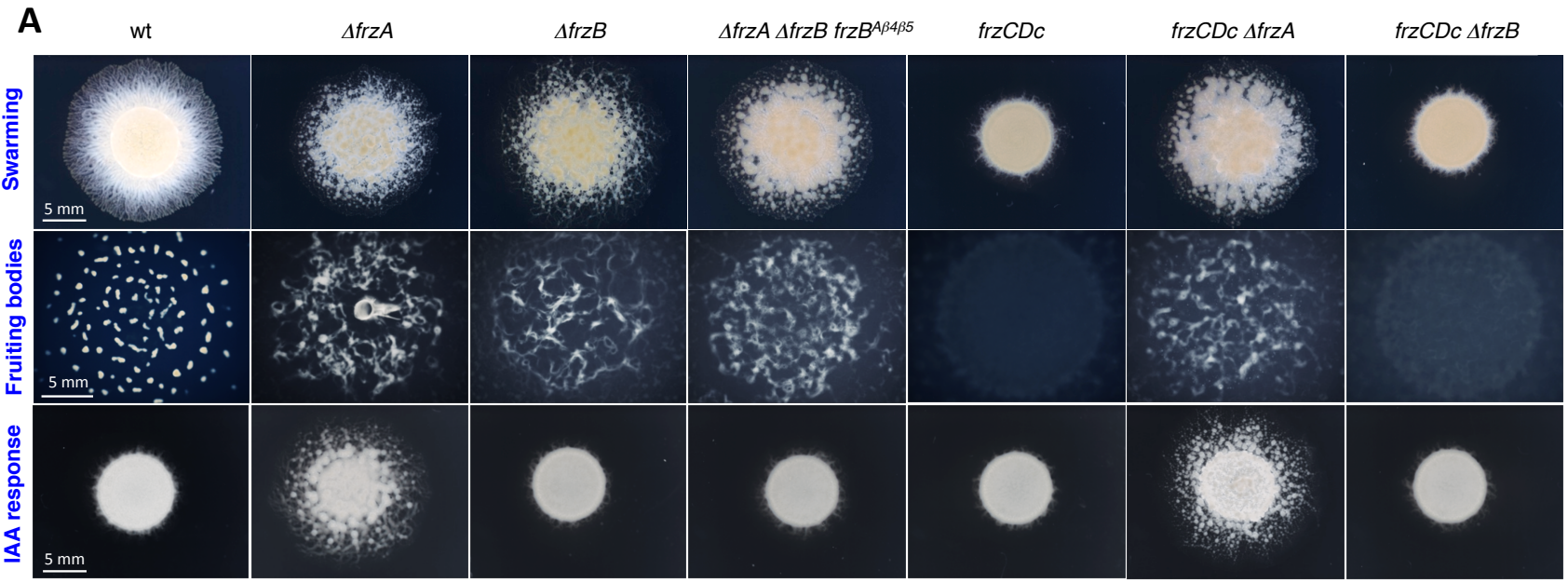
A
wt
ΔfrzA
ΔfrzB
ΔfrzA ΔfrzB frzB$^{A\beta4\beta5}$
frzCDc
frzCDc ΔfrzA
frzCDc ΔfrzB
Swarming
Fruiting bodies
IAA response
5 mm
5 mm
5 mm

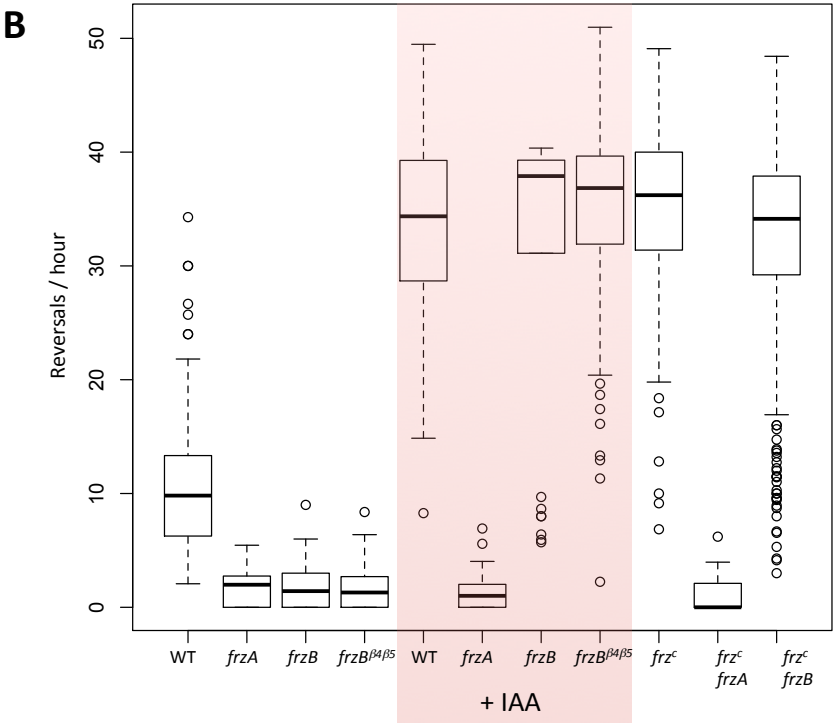
B
Reversals / hour
0
10
20
30
40
50
WT
frzA
frzB
frzB$^{\beta4\beta5}$
WT
frzA
frzB
frzB$^{\beta4\beta5}$
frz^{c}
frz^{c} frzA
frz^{c} frzB
+ IAA

A

pUT18C / pKT25	FrzA	FrzB*	FrzCD	FrzCD^Cter	FrzCD^Nter	FrzE^P5
FrzA	ND	ND	+	+	-	+
FrzB**	ND	ND	+	+	-	-
FrzCD	+	+	ND	ND	ND	ND
FrzCD^Cter	+	+	ND	ND	ND	ND
FrzCD^Nter	-	-	ND	ND	ND	ND
FrzE^P5	+	-	ND	ND	ND	ND

* in pUT18, ** in pKTN25

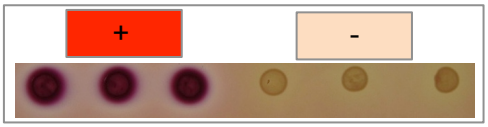

B

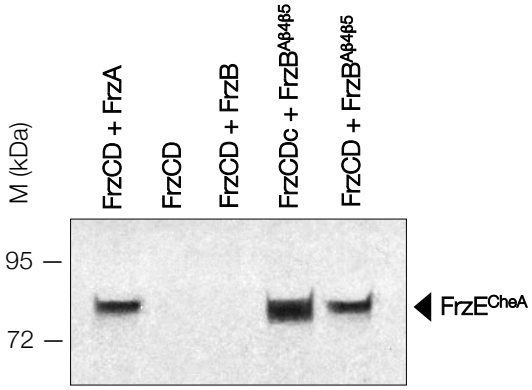

C

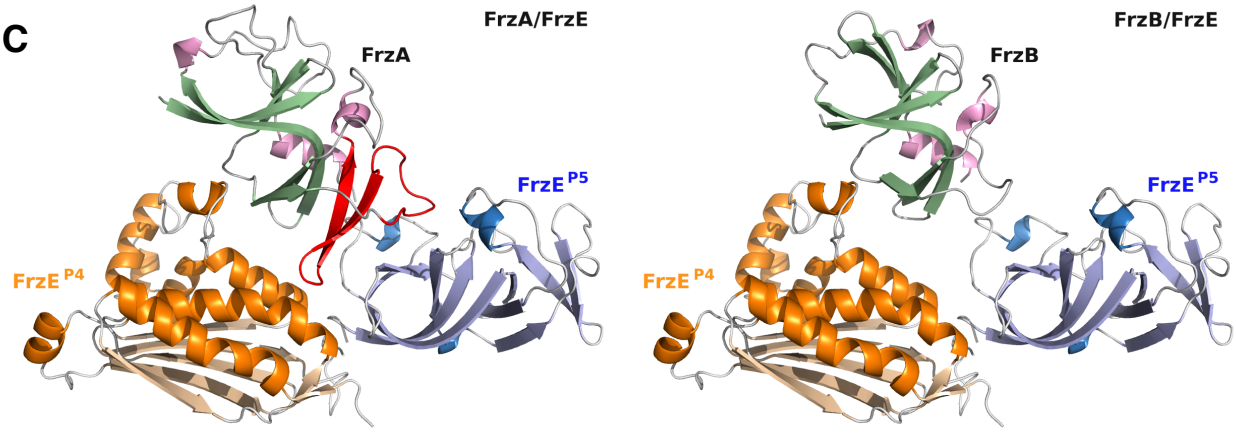

D

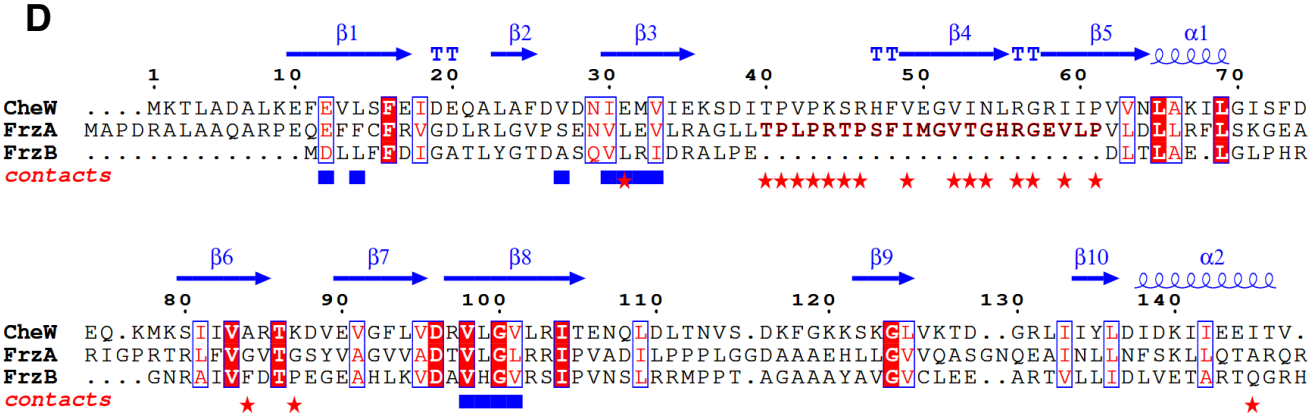

A

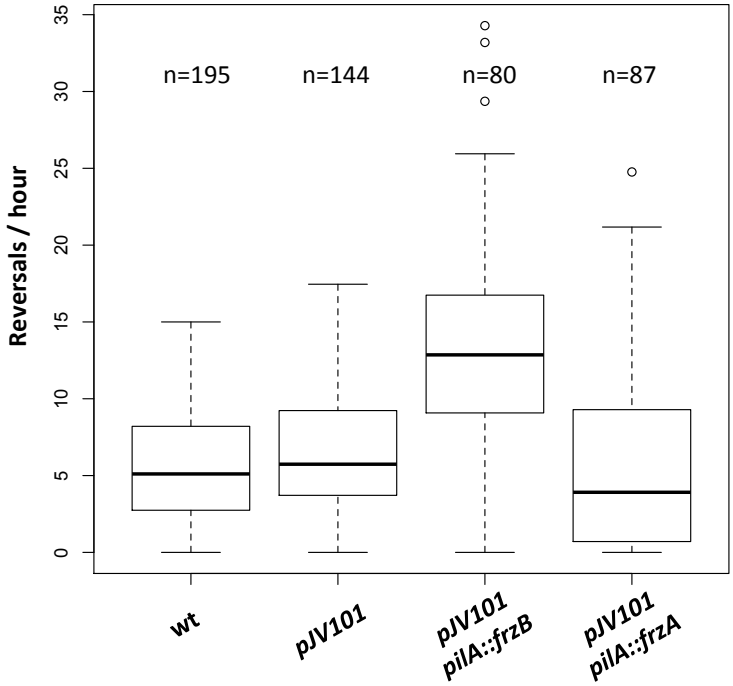

Wilcox test

	wt	pJV101	*pilA::frzB*	*pilA::frzA*
wt		0,08	2,20E-16	0,27
pJV101	0,08		2,70E-15	0,74
pilA::frzB	2,20E-16	2,70E-15		4,90E-05
pilA::frzA	0,27	0,74	4,90E-05	

B

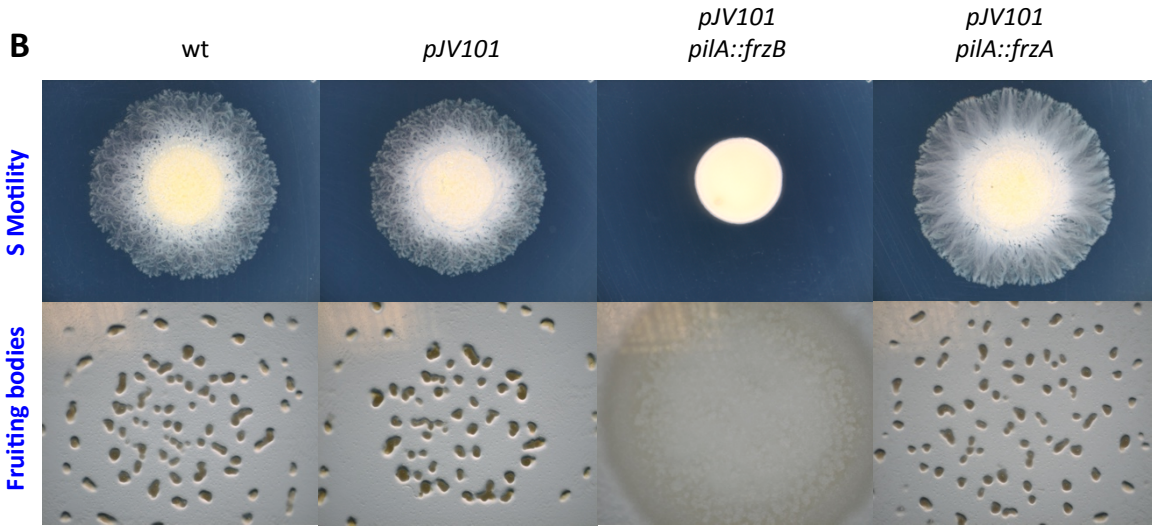

A

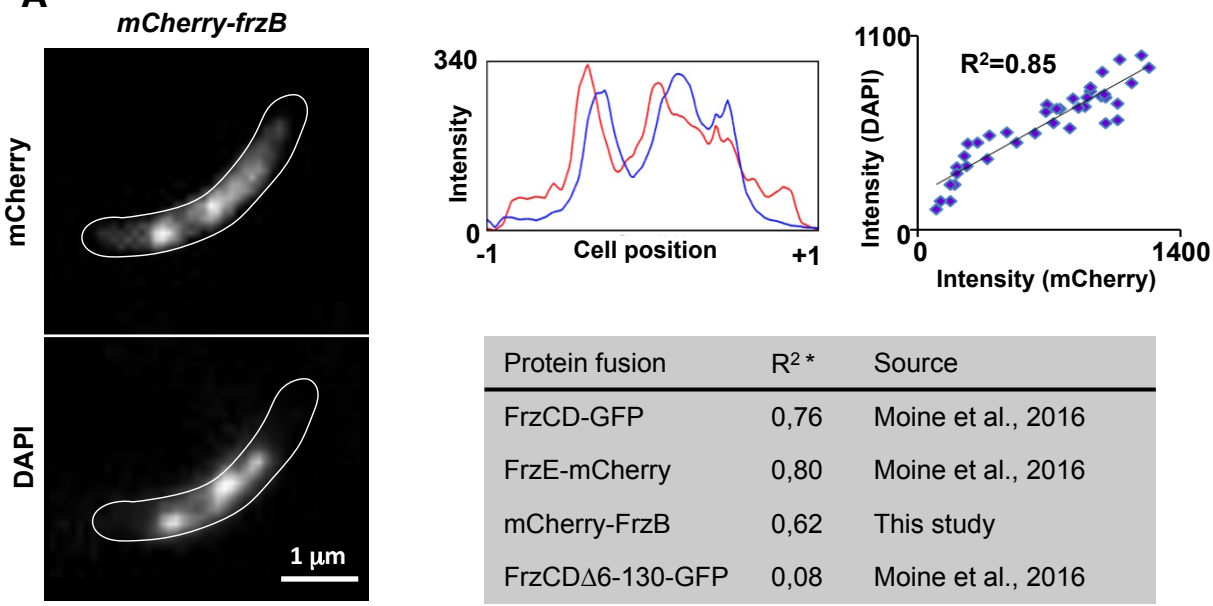

Protein fusion	R^2 *	Source
FrzCD-GFP	0,76	Moine et al., 2016
FrzE-mCherry	0,80	Moine et al., 2016
mCherry-FrzB	0,62	This study
FrzCDΔ6-130-GFP	0,08	Moine et al., 2016

* Average of 10 cells
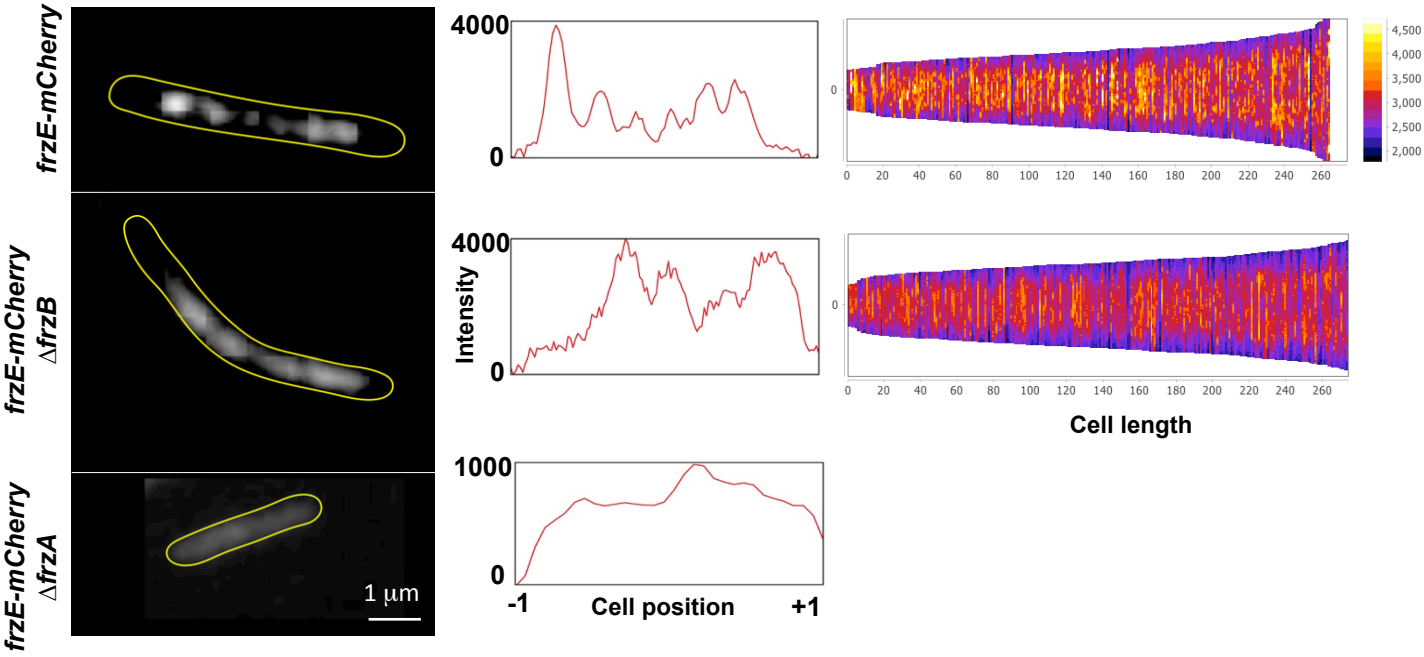
B